Development and quantitative analysis of a biosensor based on the Arabidopsis SWEET1 sugar transporter

Jihyun Park[a], Taylor M. Chavez[b], Jordan A. Guistwhite[a], Sojeong Gwon[a], Wolf B. Frommer[c,d], and Lily S. Cheung[a,1]

[a]School of Chemical and Biomolecular Engineering, Georgia Institute of Technology, Atlanta, GA 30332; [b]Department of Bioengineering, Stanford University, Stanford, CA 94305; [c]Institute for Molecular Physiology, Cluster of Excellence on Plant Sciences, Heinrich Heine Universität Düsseldorf, D-40225 Düsseldorf, Germany; and [d]Institute of Transformative Bio-Molecules, Nagoya University, Aichi 464-8601, Japan

Edited by John Patrick, School of Environmental and Life Sciences, University of Newcastle, Callaghan, NSW, Australia; received October 19, 2021; accepted December 13, 2021, by Editorial Board Member Julian I. Schroeder

SWEETs are transporters with homologs in Archeae, plants, some fungi, and animals. As the only transporters known to facilitate the cellular release of sugars in plants, SWEETs play critical roles in the allocation of sugars from photosynthetic leaves to storage tissues in seeds, fruits, and tubers. Here, we report the design and use of genetically encoded biosensors to measure the activity of SWEETs. We created a SweetTrac1 sensor by inserting a circularly permutated green fluorescent protein into the *Arabidopsis* SWEET1, resulting in a chimera that translates substrate binding during the transport cycle into detectable changes in fluorescence intensity. We demonstrate that a combination of cell sorting and bioinformatics can accelerate the design of biosensors and formulate a mass action kinetics model to correlate the fluorescence response of SweetTrac1 with the transport of glucose. Our analysis suggests that SWEETs are low-affinity, symmetric transporters that can rapidly equilibrate intra- and extracellular concentrations of sugars. This approach can be extended to SWEET homologs and other transporters.

biomolecular sensors | SWEET sugar transporters | fluorescence microscopy

Membrane transporters are crucial regulators of metabolism. In plants, sugar transporters are responsible for controlling the long-distance translocation of sugars from photosynthetic tissues to sinks like roots, seeds, and fruits. The cellular uptake and release of sugars is one of the most intensely studied processes in biochemistry and plant physiology (1).

New technologies to characterize sugar transporters in their natural environment are necessary to fully understand their contribution to plant physiology. The expression of tagged proteins helps ascertain localization and protein levels, but they do not show whether the transporters are active or idle. On the other hand, in vitro experiments with reconstituted vesicles or heterologous systems can provide affinity measurements, but they cannot capture the effect of posttranslational regulation that will arise in the original host organism.

Recently developed, genetically encoded transporter biosensors have been proposed as a way to study the function of these proteins in vivo. These biosensors consist of fusions between full-length transporters and fluorescence proteins, where the binding of the substrate to the transporter is translated into fluorescence changes (2, 3). These types of biosensors are functional and can be used to replace wild-type transporters in plants, offering the opportunity to calculate substrate movement in and out of cells in living tissues (4). Transporter biosensors could be used to visualize the routes taken by sugars from source to storage organelles and reveal bottlenecks in the allocation pathway. They could also help discern the activity of individual transporters in cells where multiple other ones are present, act as molecular phenotypes in mutagenesis screens, and help accelerate the directed evolution of transporters.

However, before transporter biosensors become widely adopted in research, two critical limitations need to be addressed. First, the design of biosensors is laborious and requires multiple rounds of optimization. Given the large number of transporters present in plant species (1), progress in the field will depend on adopting techniques that accelerate their generation. Second, it is still unclear how to reconcile fluorescence changes displayed by transporter biosensors with our molecular understanding of how transporters function.

Here, we propose a design pipeline and a mathematical framework to address both of these concerns in the context of a new sugar transporter biosensor named SweetTrac1. We constructed this biosensor from an *Arabidopsis thaliana* SWEET, a recently discovered family of transporters and the only known to facilitate the cellular release of sugars in plants (5). Our analysis indicate that SweetTrac1 may be a viable analog to the wild-type *Arabidopsis* SWEET1, as we found the biosensor to have comparable glucose influx and efflux affinities. We also present a mathematical model that allowed us to calculate the net transport rate from the fluorescence changes displayed by the biosensor. Our results highlight the potential of biosensors

Significance

Transporters are the gatekeepers of the cell. Transporters facilitate the exchange of ions and metabolites between cellular and subcellular compartments, thus controlling processes from bacterial chemotaxis to the release of neurotransmitters. In plants, transporters have key roles in the allocation of carbon to nonphotosynthetic organs. Biosensors derived from transporters have been generated to monitor the activity of these proteins within the complex environment of the cell. However, a quantitative framework that reconciles molecular and cellular-level events to help interpret the response of biosensors is still lacking. Here, we created a sugar transporter biosensor and formulated a mathematical model to explain its response. These types of models can help realize multiscale, dynamic simulations of metabolite allocation to guide crop improvement.

Author contributions: J.P., W.B.F., and L.S.C. designed research; J.P., T.M.C., J.A.G., S.G., and L.S.C. performed research; J.P. and L.S.C. analyzed data; and J.P. and L.S.C. wrote the paper.

The authors declare no competing interest.

This article is a PNAS Direct Submission. J.P. is a guest editor invited by the Editorial Board.

[1]To whom correspondence may be addressed. Email: lily.cheung@gatech.edu.

This article contains supporting information online at http://www.pnas.org/lookup/suppl/doi:10.1073/pnas.2119183119/-/DCSupplemental.

Published January 19, 2022.

to advance in vivo biochemical studies. Furthermore, our approach could be applicable to other transporters that function by an alternative access mechanism, such as the human glucose transporters (GLUTs) and sodium–glucose linked transporters (SGLTs).

Results

Generation of SweetTrac1. To create SweetTrac1, we sought to insert a circularly permutated, superfolded green fluorescent protein (cpsfGFP) between the two pseudosymmetric halves of the *Arabidopsis* SWEET1 (Fig. 1*A* and *SI Appendix*, Fig. S3)—an approach first demonstrated fruitful in the construction of AmTrac, a biosensor made from the ammonium transceptor AMT1;3 (6). Six potential insertion sites in the intracellular loop connecting the third and fourth transmembrane helices of AtSWEET1 were selected from a homology model based on the structure of the rice OsSWEET2b (7). The optimal insertion site was then identified using a yeast complementation assay in which chimeras with a cpsfGFP insertion were expressed in the *Saccharomyces cerevisiae* EBY4000 strain (8) (*SI Appendix*, Fig. S1). EBY4000 lacks all known endogenous hexose carriers, thus requiring expression of a functional glucose transporter to restore growth in media that contain glucose as the sole carbon source. In AmTrac, only fusion proteins that can still transport their substrate display a fluorescence change (6). Therefore, we selected the position after K93 in the protein, corresponding to the chimera that best restored growth in the EBY4000 strain (*SI Appendix*, Fig. S1).

The split AtSWEET1 and cpsfGFP proteins needed to be connected by two linker peptides (Fig. 1*A*), the composition of which is known to be critical for biosensor performance. For example, in AmTrac (6), modifying the linkers varied the fluorescence intensity change resulting from ammonium addition. Unfortunately, the sequence space for linkers scales with 20^n in which n is the number of amino acids in the linkers; thus, optimization remains largely empirical.

A gene library of chimeras with two- and three-amino-acid-long linkers was generated by PCR amplification of the sequence of cpsfGFP using primers containing NNK degenerate codons. The resulting DNA fragment was inserted by yeast homologous recombination into a linearized vector containing the sequence of AtSWEET1 (Fig. 1*B*). To accelerate the selection of linkers from the library, we took advantage of fluorescence-activated cell sorting (FACS) to remove nonfluorescent fusion proteins (Fig. 1*B* and *C*). We screened 450,000 cells expressing biosensor variants in three separate experiments and isolated over 900 cells with the highest level of green fluorescence.

Cells isolated by FACS were regrown in liquid media and tested for fluorescence change in response to the addition of glucose, a known substrate of AtSWEET1 (5). We chose 44 outliers with the largest fluorescence increases for sequencing. For comparison, we also randomly chose 40 negative controls from the remaining cells isolated by FACS. Some differences in the amino acid composition of linkers between these two groups were apparent (*SI Appendix*, Fig. S2), with three-amino-acid-long linkers overrepresented among the outliers. We identified biosensor candidates with the same linkers multiple times—there were only 15 unique linker combinations among the 44 outliers. This result was unexpected given the vast predicted sequence space of the library (64 million variants). We hypothesize that a combination of PCR amplification biases, low transformation efficiency, and the need to allow cells to recover and regrow following transformation may have reduced the diversity of our pool of linker variants. Future improvements in gene synthesis and yeast transformation would increase the efficiency of our approach.

A sequence comparison of the linkers in the outliers showed the prevalence of particular amino acids at each position as illustrated in Fig. 1*D*. Furthermore, statistical coupling analysis suggested that the amino acid distributions at each position were independent of one another (9); albeit, a larger sample size may be necessary to corroborate our result. This observation led us to hypothesize that better linkers may be obtained by selecting the most frequent amino acid observed at each position. Indeed, we created a new variant with the left and right linker sequences DGQ and LTR, respectively, which combined the high base fluorescence level and large change of two other candidates (Fig. 1*E* and *SI Appendix*, Fig. S3). We named this designed variant SweetTrac1.

Photophysical Characterization of SweetTrac1. We characterized the fluorescence change response of SweetTrac1 to glucose in yeast cells, where the biosensor is mainly localized to the plasma membrane but also present in the vacuole (5) (Fig. 2*A*). A spectra analysis of SweetTrac1 revealed two excitation maxima—a major peak from the deprotonated chromophore at a wavelength of ∼490 nm and a minor peak from the protonated chromophore at a wavelength of ∼410 nm. A single emission maximum was observed at a wavelength of ∼515 nm (Fig. 2*B*). The peak fluorescence intensity increased with glucose addition, while no shift in excitation and emission maxima were observed (Fig. 2*B*).

SweetTrac1 Fluorescence Response Was Correlated with Glucose Binding. To test if SweetTrac1 can also transport glucose as the wild-type AtSWEET1 does (5), we expressed the biosensor in EBY4000 and measured [^{14}C]-glucose influx. The results

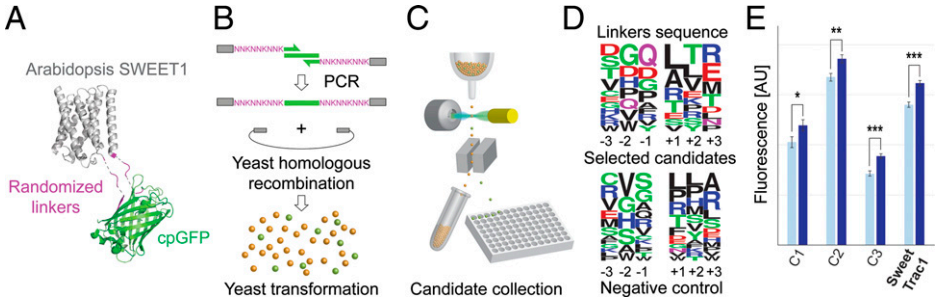

Fig. 1. Generation of the SweetTrac1 biosensor. (*A*) Representation of SweetTrac1 based on a homology model created from the structure of the rice OsSWEET2b (Protein Data Bank identifier [PDB ID] 5CTG) and cpGFP (PDB ID 3EVP). (*B* and *C*) A pool of constructs with different linkers connecting AtSWEET1 and cpsfGFP were generated with mixed-base primers and isolated by FACS. (*D*) Amino acid distribution at each linker position for constructs that showed a change in fluorescence intensity in a screen with the addition of glucose. WebLogo was created from the amino acid frequency of 15 unique linkers combinations. (*E*) Fluorescence change of the SweetTrac1 sensor (488 nm excitation, 514 nm emission) designed with the most conserved residues at each linker position, compared to the top three candidates (C1 to 3) identified during the screen. Light blue: 0 mM of glucose; dark blue: 100 mM of glucose (mean ± SE; $n = 10$; $^*P < 0.05$, $^{**}P < 0.01$, and $^{***}P < 0.001$).

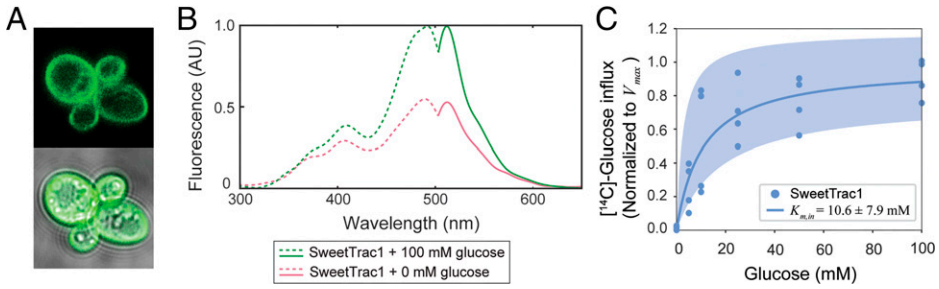

Fig. 2. Characterization of the SweetTrac1 sensor. (*A*) Localization of SweetTrac1 to the plasma membrane in yeast cells. (*B*) Normalized fluorescence excitation and emission spectra of SweetTrac1 (455 nm excitation, 530 nm emission). Dashed lines illustrate excitation and solid lines illustrate emission. (*C*) [^{14}C]-glucose influx assay for SweetTrac1 in yeast. Data were fitted to *SI Appendix*, Eq. **17**. Solid lines represent model fit, and shaded areas represent 95% CIs (coefficient reported as estimate ±95% CIs; $n = 4$; $R^2 = 0.78$).

showed that SweetTrac1 is a functional transporter that can mediate the influx of glucose (Fig. 2*C*) with kinetics similar to those reported for AtSWEET1 (5, 10), although we cannot absolutely rule out the possibility that the intramolecular insertion of cpsfGFP may have altered the stability or half-life of the transporter.

To test whether the fluorescence changes of the biosensor were associated with glucose binding, we mutated different amino acids near the substrate-binding site of SweetTrac1 (7, 11, 12). We found that mutations that abolish [^{14}C]-glucose transport (P23A, N73A, and N192A in the AtSWEET1 sequence) also abolished the fluorescence change in response to the addition of glucose, despite the biosensor retaining plasma membrane localization in yeast (Fig. 3*A* and *B* and *SI Appendix*, Fig. S4). Conversely, SweetTrac1 mutants that did not affect transport (Y179A, P45A, Y57F, D65A, and S54C) still produced a fluorescence response (Fig. 3*A* and *B*), although protein levels seemed to vary between mutants (*SI Appendix*, Fig. S4). These differences in protein levels could explain the differences in [^{14}C]-glucose between mutants (Fig. 3*A*). Overall, the results showed that SweetTrac1 responds to glucose binding; albeit, further mutagenesis experiments would be necessary to determine whether the precise molecular mechanism involves the binding of substrate per se or the disruption of interactions between the backbone amino acids triggered by substrate binding as it has been proposed for the yeast amino acid permease Gap1 (13).

Derivation of a Three-State Uniporter Model for SweetTrac1. The crystal structures of multiple bacterial homologs of SWEETs, the SemiSWEETs, show that these transporters adopt at least three states during a translocation cycle: outward-facing open, occluded, and inward-facing open (7, 11, 14). The identification of these states indicates that SWEETs follow an alternating access mechanism (14). SWEETs have also been reported to be pH independent (1, 5), thus supporting a uniport mechanism (sometimes also referred to as facilitated diffusion) (1). Based on these observations, we proposed a three-state, alternating access model for SweetTrac1 (Fig. 4*A*). In the model, E_i, E_o, and ES denote the inward-facing open, outward-facing open, and occluded bound states, respectively. The subscript i indicates inside, while o denotes outside. Six kinetic rate constants for the shifts between each configuration are denoted by k_1 to k_6.

An equation for the net transport rate (v_{io}^{net}) can be derived from this model by making four major assumptions. First, rates are determined by mass action kinetics. Second, intermediate forms of the transporter (E_i, E_o, and ES) reach quasi steady state instantaneously (15, 16). Third, each transition is in equilibrium with its reverse process. From the principle of detailed balance, the rates of the forward and reverse cycles must be equal at equilibrium if the concentrations on both sides of the membrane are to be the same. Lastly, the measured fluorescence corresponds to the concentration of the bound state (ES), which is based on the observation that the steady-state

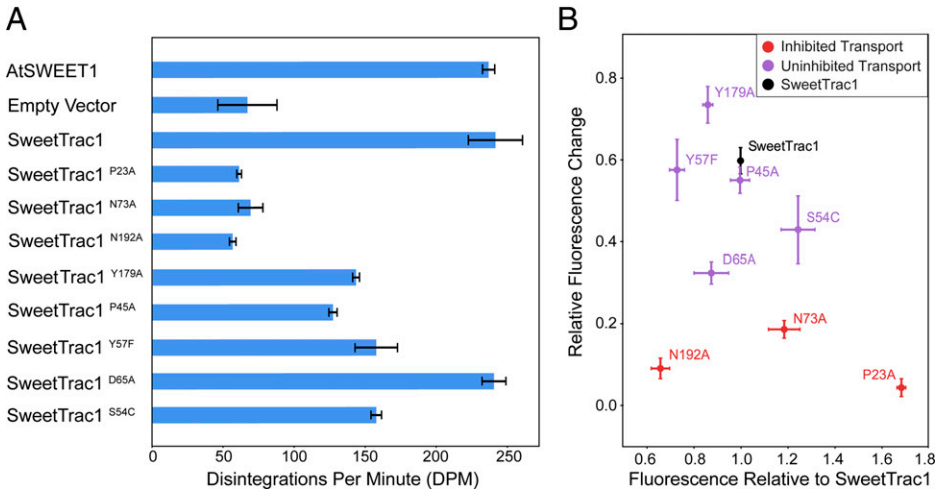

Fig. 3. SweetTrac1 mutants with abolished transport activity do not display a fluorescence response. (*A*) Radioactive uptake of 100 mM [^{14}C]-glucose by SweetTrac1 mutants in yeast (mean ± SE; $n = 3$). (*B*) Fluorescence response of SweetTrac1 and mutants to 100 mM glucose (mean ± SE; $n = 3$).

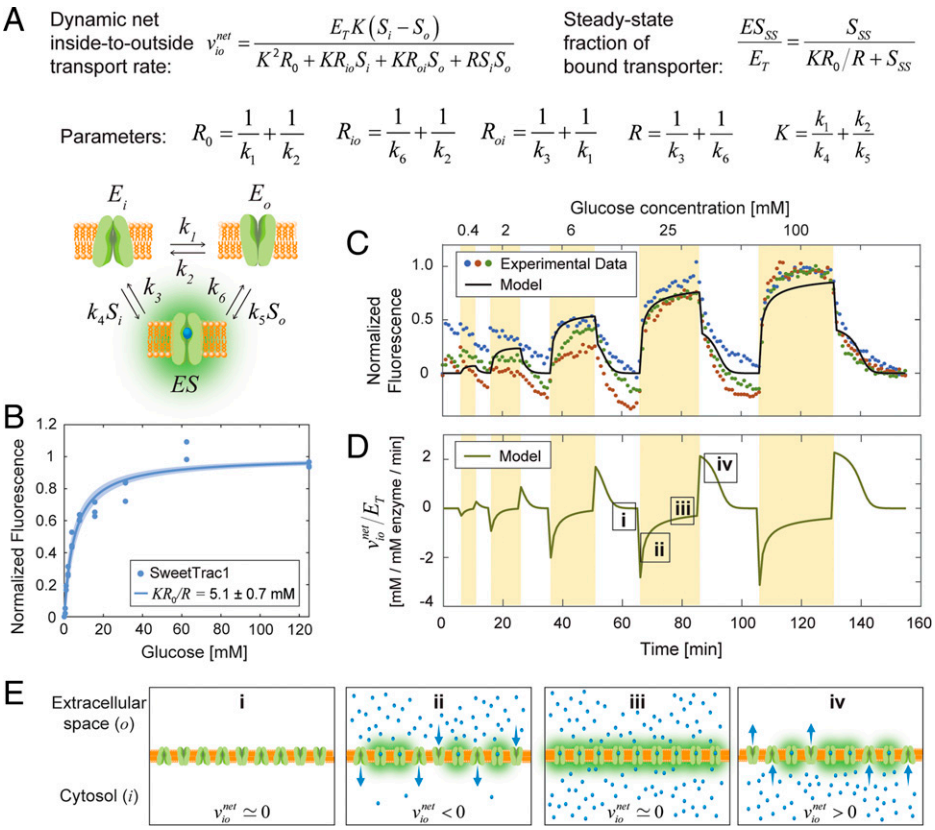

Fig. 4. Kinetic model for uniporters and analysis of SweetTrac1. (*A*) Minimal, three-state model for different states of the transporters: inside open (E_i), outside open (E_o), and substrate bound (*ES*). E_T is the total concentration of enzyme. The net transport rate and the steady-state fraction of bound transporter can be characterized by four resistance parameters (R_0, R_{io}, R_{oi}, and R) and an intrinsic dissociation constant (K). At steady state, the concentration of substrate (S_{SS}) inside (S_i) and outside (S_o) of cells are equal. (*B*) Steady-state response of SweetTrac1 measured in microplate readers. Solid line illustrates model fit for the fraction of steady-state bound transporter, and shaded areas represent 95% CIs (coefficient reported as estimate ±95% CIs; $n = 3$; $R^2 = 0.97$). (*C*) Dynamic response of SweetTrac1 measured in a commercial microfluidic device ($n = 3$ cell populations). Black line illustrates model fit ($R^2 = 0.83$). (*D*) Calculated net transport rate of glucose per mM of active enzyme. (*E*) Schematic of the SweetTrac1 transport process. The net transport rate is zero when the concentration of glucose on both sides of the membrane are both zero (*i*) or equal (*iii*). When the extracellular concentration is higher than the intracellular one, glucose enters cells, and the net transport rate is negative (*ii*). Contrarily, when the intracellular concentration of glucose is higher than the extracellular one, glucose exits cells, and the net transport rate is positive (*iv*).

fluorescence of SweetTrac1 increased with glucose addition (Fig. 2*B*). This means we consider the E_i and E_o states low fluorescence states, while *ES* is a bright state. The derivation for the net transport rate equation is detailed in *SI Appendix* following previous work (15, 16).

The net transport rate can be described in terms of an intrinsic dissociation constant K and four resistances, R, R_0, R_{io}, and R_{oi} (Fig. 4*A*). Briefly, R and R_0 are the overall resistances to a complete transport cycle by a bound and empty transporter, respectively. On the other hand, R_{io} and R_{oi} are the resistances in zero-*trans* experiments in the inside-to-outside and outside-to-inside directions, respectively (15, 16) (*SI Appendix*).

The Three-State Model Recapitulated the Dynamics of SweetTrac1. The steady-state fraction of the bound transporter can be described by a simple group of parameters, KR_0/R (Fig. 4*A*). This group represents the half-saturation concentration at steady state, when the intra- and extracellular concentrations of the substrate have equalized ($S_{SS} = S_i = S_o$). Here, we will refer to this group as the equilibrium exchange constant, which can be used to describe the concentration-dependent response of our biosensor to sugars in microplate readers (Fig. 4*B*). SweetTrac1's equilibrium exchange constant for glucose was 5.1 ± 0.7 mM, meaning that half of the biosensors were in their *ES* state at this concentration.

Our model recapitulated the reversible and concentration-dependent behavior of SweetTrac1. Yeast cells expressing the biosensor were imaged in a fluorescence confocal microscope with the help of a commercially available microfluidic device. The device allowed the immobilization of the cells in the field of view and rapid changes in the extracellular concentration of glucose (Fig. 4*C*). To estimate the rate constants k_1 to k_6 (*SI Appendix*, Table S1), we numerically solved the system of four differential equations describing the accumulation of S_i, E_i, E_o, and *ES* (*SI Appendix*). We used this solution to fit both the steady-state fluorescence response of SweetTrac1 in microplates and the dynamic response in the microfluidic device (Fig. 4 *B* and *C*). It is worth noting that we had a large number of parameters in our model and experimental noise. Despite our extensive search, we cannot exclude the existence of an alternative set of parameters that leads to a global minimum.

The fitted model allowed us to calculate the net glucose transport rate (Fig. 4*D*). Per the definition of the net transport rate (Fig. 4*A*), its value should be zero in the absence of substrates (Fig. 4 *E*, *i*). When intracellular concentrations are lower than the extracellular ones, substrates enter cells, and the net transport rate has negative values (Fig. 4 *E*, *ii*). Conversely, when the intracellular concentrations are higher than the extracellular ones, substrates exit, and the net transport rate is positive (Fig. 4 *E*, *iv*). If substrates accumulate intracellularly to

concentrations equal to those outside, the net transport rate will be zero (Fig. 4 *E*, *iii*), but in this case, SweetTrac1 will be in its bound and bright state.

The model fit of the dynamic response appeared better at high glucose concentrations than at low ones (Fig. 4*D*). Unfortunately, focal drift was common in our experiments. Moreover, the levels of plasma membrane–localized proteins are generally low (compared with cytosolic proteins), even under strong promoters, which made imaging SweetTrac1 with the temporal resolution necessary for parameter estimation susceptible to photobleaching. To reduce the number of negative values, we used the fluorescence of the biosensor at the end of the experiment for normalization. This resulted in a poor fit at the initial low concentrations of glucose. To fully understand the departure between the model and the experimental data, we exposed cells expressing SweetTrac1 to 2 or 6 mM of glucose and quantified the fluorescence of SweetTrac1 using a microplate reader (*SI Appendix*, Fig. S5). A visual inspection of these results suggested a better agreement with the model than the dynamic data showed (Fig. 4*C*); albeit, the signal-to-noise ratio and goodness of fit were low. This could be due to the fact that microplate readers typically do not suffer from the same focal drift and photobleaching as confocal microscopes, but they are often less sensitive.

The parameters estimated in our model agreed with experimentally measured glucose influx for SweetTrac1. In a zero-*trans* influx experiment, the intracellular concentration of substrate is zero, and the net transport rate equation reduces to a simpler form ($S_i = 0$) that depends on the extracellular concentration of substrate and the group of parameters KR_0/R_{oi} (*SI Appendix*, Eq. 17). Here, we refer to this group as the zero-*trans* influx constant, sometimes referred to in the literature as the Michaelis constant (K_m) for influx assays. We found the value of the zero-*trans* influx constant for SweetTrac1 calculated from the fluorescence data to be 3.8 ± 1.1 mM, comparable to the value of 10.6 ± 7.9 mM we obtained for SweetTrac1 from [^{14}C]-glucose influx assays (Fig. 2*C*). Both values were also close to the 9 mM reported in the literature for AtSWEET1 (5, 10). The discrepancy between our imaging and radiolabeled influx experiments could be due to partial localization of SweetTrac1 to the endoplasmic reticulum or intracellular vesicles in which it still showed a fluorescence response but could not alter the cellular influx of glucose. This partial mislocalization of overexpressed heterologous transporters is a well-recognized phenomenon in yeast not particular to SweetTrac1 (17). Nevertheless, our results intimated that SweetTrac1 generated a fluorescence response within the same millimolar concentrations relevant for the wild-type transporter.

The Three-State Model Revealed the Existence of a Theoretical Optimum. It has been suggested that uniporters like SWEETs have an optimal affinity that parallels the physiological concentration of substrates at which they function (18). For efflux, when the extracellular substrate affinity is higher than the intracellular concentration of substrate, the net efflux rate will be reduced by the lack of substrate. Conversely, efflux could also be reduced when the affinity is considerably lower than the intracellular concentration. When both the transporter's inward-facing and outward-facing binding sites are saturated with substrate, the unidirectional inside-to-outside and outside-to-inside transport rates will have similar magnitudes, and the net efflux rate will consequently decrease.

We performed a computational analysis of our model to identify the conditions that lead to the optimal net transport rate. We explored a wide range of values of the rate constants k_1 to k_6 and found that the maximum net transport rate depends on the interplay between the concentration gradient, the equilibrium exchange constant, and an asymmetry ratio (Fig. 5*A*). The asymmetry ratio is mathematically equal to R_{io}/R_{oi} (15). Maximum net transport occurred when the substrate concentrations and equilibrium exchange constants were within the same order of magnitude. Furthermore, a symmetric transporter could achieve higher net transport rates than an asymmetric one at any substrate concentration (Fig. 5*A*).

Our three-state model suggested that AtSWEET1 may be a symmetric transporter. Uniporters are often kinetically asymmetric for a biological purpose (15). For instance, in red blood cells, GLUT1 is asymmetric, with an asymmetry ratio of 18.75 to 37.50. This ratio indicates that GLUT1 greatly favors influx as opposed to efflux (19). It has been proposed that its sided behavior allows glucose-exhausted cells to rapidly replenish themselves upon recirculation into a high glucose environment, while glucose release would be delayed when transiting low glucose environments (20). For SweetTrac1, we were able to estimate an asymmetry ratio of 1.2 ± 0.2 from the fluorescence data, indicating that AtSWEET1 is a symmetric transporter and thus would not buffer changes in intracellular sugar concentrations like GLUT1. We corroborated this prediction experimentally with [^{14}C]-glucose influx and efflux assays on AtSWEET1 and found a comparable asymmetry ratio of 1.0 ± 1.2 (Fig. 5 *B* and *C*).

Furthermore, in the absence of substrate, the model suggested that SweetTrac1 favors the inward-open state instead of the outward-open state ($k_1/k_2 = 0.7$). This ratio indicated that the inward-open state E_i is roughly 1.3 times more stable than the outer-open state E_o, which aligns with molecular simulations of LbSemiSWEET in the literature (11).

Given the equilibrium exchange constant and asymmetry ratio of SweetTrac1, we propose that SWEETs have evolved to maximize net sugar transport at high concentrations, such as those in plants where glucose levels in the apoplasmic fluid have been found to reach tens of millimoles (21).

Discussion

In this work, we generated SweetTrac1, a biosensor to study sugar allocation in plants. Our FACS-based approach could accelerate the development of biosensors, although some limitations are worth noting. When generating SweetTrac1, our screen for possible candidates was small compared with the theoretical number of possible variants. We cannot rule out that we may find better linkers upon further experimentation. In addition, further improvements to our strategy such as the use of high-throughput sequencing of pooled candidates to increase the number of linkers analyzed may help optimize their composition. Nevertheless, our positive results suggest that exhaustive coverage of the initial gene library may not be necessary, which could be exploited to speed the design process. Furthermore, our work showed that using an organism's endogenous proteins as scaffolds is a valuable approach to produce biosensors that function within physiological ranges.

We accompanied our biosensor with a mathematical model to explain its response quantitatively. We used a unique method to study the structural transitions of membrane transporters without the need for radiolabeled or fluorescently tagged substrates. We estimated the rate constants k_1 to k_6, describing how SweetTrac1 (and possibly AtSWEET1) shifts between conformations. To our knowledge, the estimation of the individual rate constants (not only the combined K and R parameters) has not been performed in this way before.

We also described several experimental challenges that complicated the quantitative analysis of fluorescence biosensors, namely protein mislocalization, photobleaching, and focal drift. To account for these effects, we produced 95% CIs for all data fits and propagated errors to the calculated equilibrium exchange constant and asymmetry ratio. Very importantly, our

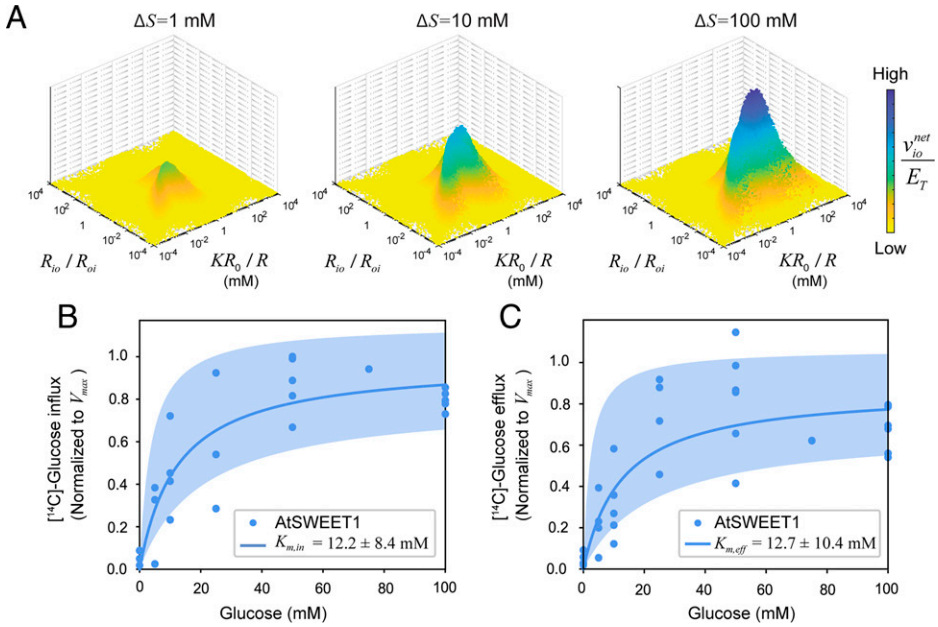

Fig. 5. Kinetics of glucose transport in AtSWEET1. (*A*) Effect of parameter values on the net transport rate at different concentration gradients (Δ*S*) in which S_o is set at 0.01 mM. (*B*) [^{14}C]-glucose influx assay for AtSWEET1 in yeast. Data were fitted to *SI Appendix*, Eq. **17** (n = 5; R^2 = 0.76) (*C*) [^{14}C]-glucose efflux assay for AtSWEET1 in yeast. Data were fitted to *SI Appendix*, Eq. **18** (n = 6; R^2 = 0.66). (*B* and *C*) Solid lines represent model fit, and shaded areas represent 95% CIs (coefficients reported as estimates ±95% CIs).

conclusion that SweetTrac1 is a high-capacity and near symmetric transporter is not substantially altered when accounting for extreme values of the estimated parameters k_1 to k_6.

Additionally, it is worth pointing out that in both our influx and efflux experiments, rates appeared to decrease from 50 to 100 mM glucose (Fig. 5 *B* and *C*). This behavior has not been noted in previous kinetics studies of AtSWEET1 (5, 10). The decrease could be an artifact produced by osmotic effects, as the zero-*trans* experiments require preincubating the yeast cells in media with either 0 or 100 mM glucose and a rapid switch to the opposite concentration, resulting in cell shrinkage. Alternatively, the decrease in transport rates at 100 mM could result from an unexplored form of substrate regulation. For our analysis of the fluorescence response of SweetTrac1, if not all the biosensors are bound to glucose at 100 mM or if there is an additional dim, less active state that only occurs around 100 mM, there could be an error of up to 8% in our calculations of the fraction of glucose-bound SweetTrac1.

Our overall analysis suggested that the physiological function of AtSWEET1 may be to equilibrate the intra- and extracellular concentrations of sugars rapidly. Given the low affinity and symmetry predicted by our biosensor and measured in AtSWEET1 (Figs. 4*B* and 5 *B* and *C*), we expect AtSWEET1 to allow high net influx and efflux rates in planta. This will rapidly equalize sugar concentrations on both sides of the membrane, unlike the concentration buffering attributed to GLUT1 in red blood cells (19, 20). While the physiological role of AtSWEET1 is unclear, its maize homolog was shown to facilitate the uptake of glucose into subsidiary cells, where glucose acts as a feedback inhibitor of stomatal opening (22). In this context, by allowing the intracellular concentration of glucose to equilibrate with the extracellular one quickly, ZmSWEET1b may help speed the response of the feedback mechanism. In general, SWEETs can be considered uniporters that, given their low affinity, are less likely to saturate at the high sugar concentrations possible in plant tissues (21, 23).

Sugar transporters like SWEETs play critical roles in many physiological processes, notably facilitating the efflux of sucrose out of leaf cells—as the first step for phloem loading—and in pathogen infection (5, 24). This fact makes SWEETs important biotechnology targets. For example, genomic editing promoters of SWEET genes in rice conferred resistance to bacterial blight (25). Crop improvement could be made even faster with the help of biosensors like SweetTrac1 and computational models to select target genes for modification (26).

More generally, we are in the midst of a high-throughput revolution in which plant genomes are becoming readily available. Approximately a tenth of those genomes encode transport proteins (27). As we continue to identify transporters in large numbers, we will need new functional characterization methods that match the speed of current sequencing techniques. We will also need ways to study transporters in their physiological context, associated with their regulatory proteins and metabolic pathways (4, 28). Biosensors could be important tools to facilitate such studies and for the development of computational models. Our work demonstrated the potential of biosensors in collecting quantitative data nondestructively. Future biosensors like SweetTrac1 could help answer systems-level questions on substrate competition, concentration robustness, and more.

Materials and Methods

DNA Constructs. The *Arabidopsis* SWEET1 (At1g24300) was used as the basis for generating the SweetTrac1 sensor. All sequences were cloned into the entry vector pDRf1-GW for yeast expression (29) through Gateway cloning (Invitrogen).

For construction of the SweetTrac1 library, an XbaI restriction site was inserted into position 93 of the AtSWEET1 protein. The modified pDRf1-SWEET1 plasmid was then linearized with XbaI and gel purified. Mixed-base primers, in which the linkers coding sequences were randomized using NNK degenerate codons, were used to PCR amplify the sequence of cpsfGFP. NNK encodes for 32 codons: 20 amino acids and 1 stop codon. The linearized pDRf1-SWEET1 vector and cpsfGFP fragments were ligated via homologous recombination in *S. cerevisiae*.

The final SweetTrac1 sensor contains the coding sequence of cpsfGFP, flanked by the left and right amino acid linkers DGQ and LTR, respectively. The linkers and cpsfGFP were inserted into amino acid position 93 of AtSWEET1 (*SI Appendix*, Fig. S3).

Yeast Transformation and Sorting. The SWEET1-cpsfGFP fusion library was transformed in *S. cerevisiae* using the lithium acetate method (30). Cells were plated on solid synthetic minimal medium supplemented with 2% agar, 2% maltose, and auxotrophic requirements. After 24 h, yeast cells were recovered by rinsing agar plates with liquid synthetic minimal medium supplemented with 2% maltose and auxotrophic requirements. Cells were sorted in a FACS Aria II (BD Biosciences). Fluorophore was excited using a 488-nm laser line, and emission was collected with a 530/30-nm filter set. Our initial attempts at sorting cells into 96-well plates with liquid synthetic minimal medium did not return viable cultures; instead, sorting cells into solid synthetic minimal medium proved fruitful. A total of ~450,000 cells were screened over three independent experiments, and over 900 cells (0.2%) with the highest level of green fluorescence were isolated for further testing.

To identify chimeras that exhibit a fluorescence change with the addition of substrate, colonies were regrown overnight in 96-well blocks with yeast extract peptone medium supplemented with 2% maltose, washed thrice with deionized water, and resuspended in synthetic minimal medium supplemented only with auxotrophic requirements. The fluorescence intensity of each culture (at an excitation wavelength of 488 nm and emission wavelength of 514 nm) was recorded before and after the addition of 100 mM glucose using a Tecan M1000 Pro plate reader. Plasmids from 44 colonies that exhibited a statistically significant change in fluorescence intensity with the addition of glucose were recovered and sequenced. An additional 40 colonies were randomly selected from the remaining pool and sequenced for comparison (*SI Appendix*, Fig. S1). The frequency of different amino acids in unique linkers is illustrated with the web-based application WebLogo (31).

Other supplemental materials and methods are available in the *SI Appendix*.

Data Availability. The plasmid for SweetTrac1 has been deposited in Addgene (ID code 169083). All other study data are included in the article and/or *SI Appendix*.

ACKNOWLEDGMENTS. We thank Cindy Ast and Mark P. Styczynski for helpful discussions and comments on the manuscript. This work was supported by NSF Grants 1401855 and 1942722 to L.S.C. Contributions by W.B.F. were supported by the Deutsche Forschungsgemeinschaft (German Research Foundation) under Germany's Excellence Strategy (EXC-2048/1) Project Identification 390686111 as well as the Alexander von Humboldt Professorship.

1. L.-Q. Chen, L. S. Cheung, L. Feng, W. Tanner, W. B. Frommer, Transport of sugars. *Annu. Rev. Biochem.* **84**, 865–894 (2015).
2. C. Ast *et al.*, Ratiometric Matryoshka biosensors from a nested cassette of green- and orange-emitting fluorescent proteins. *Nat. Commun.* **8**, 431 (2017).
3. C.-H. Ho, W. B. Frommer, Fluorescent sensors for activity and regulation of the nitrate transceptor CHL1/NRT1.1 and oligopeptide transporters. *eLife* **3**, e01917 (2014).
4. M. Geisler, Seeing is better than believing: Visualization of membrane transport in plants. *Curr. Opin. Plant Biol.* **46**, 104–112 (2018).
5. L.-Q. Chen *et al.*, Sugar transporters for intercellular exchange and nutrition of pathogens. *Nature* **468**, 527–532 (2010).
6. R. De Michele *et al.*, Fluorescent sensors reporting the activity of ammonium transceptors in live cells. *eLife* **2**, e00800 (2013).
7. Y. Tao *et al.*, Structure of a eukaryotic SWEET transporter in a homotrimeric complex. *Nature* **527**, 259–263 (2015).
8. R. Wieczorke *et al.*, Concurrent knock-out of at least 20 transporter genes is required to block uptake of hexoses in *Saccharomyces cerevisiae*. *FEBS Lett.* **464**, 123–128 (1999).
9. N. Halabi, O. Rivoire, S. Leibler, R. Ranganathan, Protein sectors: Evolutionary units of three-dimensional structure. *Cell* **138**, 774–786 (2009).
10. N. Kuanyshev *et al.*, Identification and analysis of sugar transporters capable of co-transporting glucose and xylose simultaneously. *Biotechnol. J.* **16**, e2100238 (2021).
11. N. R. Latorraca *et al.*, Mechanism of substrate translocation in an alternating access transporter. *Cell* **169**, 96–107.e12 (2017).
12. Y. Xu *et al.*, Structures of bacterial homologues of SWEET transporters in two distinct conformations. *Nature* **515**, 448 (2014).
13. K. Ghaddar *et al.*, Substrate-induced ubiquitylation and endocytosis of yeast amino acid permeases. *Mol. Cell. Biol.* **34**, 4447–4463 (2014).
14. J. Wang *et al.*, Crystal structure of a bacterial homologue of SWEET transporters. *Cell Res.* **24**, 1486–1489 (2014).
15. W. D. Stein, "Facilitated diffusion: The simple carrier" in *Transport and Diffusion Across Cell Membranes*, W. D. Stein, Ed. (Academic Press, 1986), pp. 231–361.
16. W. D. Stein, W. R. Lieb, A necessary simplification of the kinetics of carrier transport. *Isr. J. Chem.* **11**, 325–339 (1973).
17. J. M. Villalba, M. G. Palmgren, G. E. Berberián, C. Ferguson, R. Serrano, Functional expression of plant plasma membrane H(+)-ATPase in yeast endoplasmic reticulum. *J. Biol. Chem.* **267**, 12341–12349 (1992).
18. E. Bosdriesz *et al.*, Low affinity uniporter carrier proteins can increase net substrate uptake rate by reducing efflux. *Sci. Rep.* **8**, 5576 (2018).
19. R. Bloch, Human erythrocyte sugar transport. Kinetic evidence for an asymmetric carrier. *J. Biol. Chem.* **249**, 3543–3550 (1974).
20. A. Carruthers, J. DeZutter, A. Ganguly, S. U. Devaskar, Will the original glucose transporter isoform please stand up! *Am. J. Physiol. Endocrinol. Metab.* **297**, E836–E848 (2009).
21. J. A. Abelenda *et al.*, Source-sink regulation is mediated by interaction of an FT homolog with a SWEET protein in potato. *Curr. Biol.* **29**, 1178–1186.e6 (2019).
22. H. Wang *et al.*, A subsidiary cell-localized glucose transporter promotes stomatal conductance and photosynthesis. *Plant Cell* **31**, 1328–1343 (2019).
23. A. Shammai *et al.*, Natural genetic variation for expression of a SWEET transporter among wild species of *Solanum lycopersicum* (tomato) determines the hexose composition of ripening tomato fruit. *Plant J.* **96**, 343–357 (2018).
24. L.-Q. Chen *et al.*, Sucrose efflux mediated by SWEET proteins as a key step for phloem transport. *Science* **335**, 207–211 (2012).
25. R. Oliva *et al.*, Broad-spectrum resistance to bacterial blight in rice using genome editing. *Nat. Biotechnol.* **37**, 1344–1350 (2019).
26. J. Kromdijk *et al.*, Improving photosynthesis and crop productivity by accelerating recovery from photoprotection. *Science* **354**, 857–861 (2016).
27. M. H. Saier Jr., Q. Ren, The bioinformatic study of transmembrane molecular transport. *J. Mol. Microbiol. Biotechnol.* **11**, 289–290 (2006).
28. H. Kitano, Systems biology: A brief overview. *Science* **295**, 1662–1664 (2002).
29. D. Loqué, S. Lalonde, L. L. Looger, N. von Wirén, W. B. Frommer, A cytosolic transactivation domain essential for ammonium uptake. *Nature* **446**, 195–198 (2007).
30. R. H. Schiestl, R. D. Gietz, High efficiency transformation of intact yeast cells using single stranded nucleic acids as a carrier. *Curr. Genet.* **16**, 339–346 (1989).
31. G. E. Crooks, G. Hon, J. M. Chandonia, S. E. Brenner, WebLogo: A sequence logo generator. *Genome Res.* **14**, 1188–1190 (2004).